Proceedings of the SPIE Conference on Medical Imaging, San Diego, USA, **6144** (3), p4W1-4W12

Quantitative comparison of delineated structure shape in radiotherapy

G.J. Price and C.J. Moore

Developing Technologies – Radiotherapy, North Western Medical Physics,
Christie Hospital, Manchester, UK

ABSTRACT

There has been an influx of imaging and treatment technologies into cancer radiotherapy over the past fifteen years. The result is that radiation fields can now be accurately shaped to target disease delineated on pre-treatment planning scans whilst sparing critical healthy structures. Two well known problems remain causes for concern. The first is inter- and intra-observer variability in planning scan delineations, the second is the motion and deformation of a tumour and interacting adjacent organs during the course of radiotherapy which compromise the planned targeting regime. To be able to properly address these problems, and hence accurately shape the margins of error used to account for them, an intuitive and quantitative system of describing this variability must be used.

This paper discusses a method of automatically creating correspondence points over similar non-polar delineation volumes, via spherical parameterisation, so that their shape variability can be analysed as a set of independent one dimensional statistical problems. The importance of 'pole' selection to initial parameterisation and hence ease of optimisation is highlighted, the use of sparse anatomical landmarks rather than spherical harmonic expansion for establishing point correspondence discussed, and point variability mapping introduced. A case study is presented to illustrate the method. A group of observers were asked to delineate a rectum on a series of time-of-treatment Cone Beam CT scans over a patient's fractionation schedule. The overall observer variability was calculated using the above method and the significance of the organ motion over time evaluated.

Keywords: radiotherapy, spherical parameterisation, spherical harmonics, shape description, shape analysis, rectum, cone beam tomography

1. INTRODUCTION

The aim of radiotherapy is to deliver targeted radiation in small doses at planned intervals to an explicitly identified region in a manner that eradicates all cancer cells whilst maximally sparing surrounding healthy tissues. To do this beams of radiation are collimated to match the projected shape of a tumour from different directions and then applied sequentially. Such 'fractionated' treatments are designed to exploit the potential for healthy cells to recover from radiation exposure more quickly than diseased cells - this is the biological basis for radiotherapy. However, some healthy cells are inevitably destroyed during treatment and a balance must be struck between ensuring that all cancerous cells receive the prescribed tumourcidal dose and minimizing normal tissue complications.

The planning and review of a treatment increasingly relies on reconstructive, 3D digital imaging of the patient to reveal the size, shape and location of a tumour within the body. Common imaging technologies are X-ray Computerised Tomography (CT) and Magnetic Resonance Imaging (MRI). These map physical tissue characteristics (attenuation and primarily proton density respectively) but do not directly differentiate diseased and healthy cells, i.e. tumours often look just like adjacent healthy tissues. In addition there are imaging artefacts and performance limitations so that a tumour target, particularly one that does not correspond to an organ boundary, is often ill defined. Furthermore, pre-treatment planning scans cannot reveal the actual movements, deformations and radiation response of the target tumour and interacting adjacent Organs At Risk (OAR) that will take place during the many days, potentially weeks, of treatment. The desire to improve patient setup and

Copyright 2006 Society of Photo-Optical Instrumentation for Engineers
This paper was published in SPIE proceedings 6144 and is made available as an electronic reprint with permission of SPIE. One print or electronic copy may be made for personal use only. Systematic or multiple reproduction, distribution to multiple locations via electronic or other means, duplication of any material in this paper for a fee or commercial purposes, or modification of the content of the paper are prohibited.

tumour targeting in this context has spurred the recent adoption of kilo-voltage X-ray imaging in the treatment room, most notably in the form of wide field Cone Beam Tomography (CBT).

It is clear that during the course of treatment planning and delivery errors can accrue that could, if unaccounted for, result in the radiation dose being incorrectly delivered. Failure to ensure that all of the target volume receives the whole prescribed dose can cause the radiobiological failure of the entire treatment, whereas excessively exposing healthy tissue can have serious short and long term side effects. Two of the main error sources are widely acknowledged to be inter- and intra-observer variability in delineating the target and nearby OAR[1-4] and the involuntary internal motion of a patient's organs relative to the set-up markers used to position a patient at each treatment fraction[5-8].

Presently the uncertainties described above are accounted for by the addition of an 'error' margin to the delineated clinical target volume (CTV), a process that in effect inflates the CTV into a planning target volume (PTV) according to some expert clinical protocol[9-13]. The margins are intentionally large in order to avoid the risk of treatment failure described above. In fact the risk of treatment failure as a result of organ shape change greater than the imposed margins is of current concern, as highlighted by Roach in his editorial regarding De Crevoisier's paper on prostate treatment failure using intensity modulated radiotherapy (IMRT)[14, 15]. Large margins, however, also mean large volumes of interspersed healthy tissue are exposed with the associated health implications. Ideally, the margins would be sculpted to accurately reflect the observed variability rather than applying bulk expansions about the CTV. In order to be able to accurately shape a margin, however, it is necessary to be able to first quantitatively measure the nature of the variability.

At the Christie Hospital many patients are now receiving time of treatment CBT scans over some or all of their fractionation schedule[16] using an Elekta Synergy treatment machine specifically designed for image guided radiotherapy. This provides a wealth of data that may be used to quantify the inter-fraction motion of both target volumes and OAR. The segmentation of regions from these images is subject to observer variability, but with accurate knowledge of the nature of this variability the significance of any changes as a function of time can be assessed. An accurate knowledge of the observer variability is also a powerful tool to help in the creation and modification of delineation protocols.

Delineations are commonly compared via their total enclosed volume. This measure is literally a variability statistic that, like the dose volume histogram, does not provide any data about the underlying spatial distribution of changes i.e. the location of the variability. This paper seeks to show how shape description techniques can be applied in radiotherapy to quantitatively describe the spatial variability of an object's *shape*.

2. SHAPE DESCRIPTION

There are a myriad of different techniques that have been proposed to parameterize both two and three dimensional shapes (see[17-19] and references therein). Descriptors fall into two basic camps, those that allow the recovery of the object's shape from the descriptors and those that don't. In order to be useful in a radiotherapy setting, the variability in structures delineated on medical images need to be presented in a manner that enables meaningful and quantitative conclusions to be drawn about the nature of the variability. This essentially precludes the use of non-recoverable descriptors that, whilst giving some quantitative dissimilarity measure between objects, do not inform the user in an intuitive way of the location and magnitude of any variability.

The intuitive method of comparing like shapes, i.e. generic shapes that resemble each other but show significant variation, is to establish correspondence points on the shapes and analyse the spatial variability of these points. This approach is the basis of the two dimensional Point Distribution Model (PDM) of Cootes *et. al.*[20]. Initially these correspondence points may be established by manually placing landmarks in the image data. However, when comparing shapes without clear landmarks, it is necessary to establish some automatic way of marking correspondence points on similar shapes. Caunce and Taylor[21] extended the work of Cootes *et. al.* to three dimensions, using image processing techniques to directly create correspondence points in volumetric MRI datasets. These techniques are not applicable to the genus zero closed surfaces created by delineation (see Section 3). The genus of a surface is the maximum number of simple closed curve cuts that can be made in

it without rendering it disconnected, roughly reflecting the number of holes through it. Genus zero surfaces are also known as sphere or star like surfaces.

Remeijer *et. al.*[22] and Price and Moore[23] have both described a simple polar comparison method, where the radial distance from some point within a segmented medical image structure to its surface is expressed as a function over a sphere. Correspondence between surface points is immediately established as a function of the polar and azimuthal angles. For non-polar shapes, however, this method is not applicable as the distance from the origin of the spherical polar coordinate system to the surface of the structure is not a single valued function.

Deurloo *et. al.*[24] create a mean shape through scoring the voxels that fall within each delineation on the dataset and isosurfacing this matrix at the 50% value. Correspondence points are then assumed to be established by projecting surface normals from the mean shape to each of those to be matched. Kelemen *et. al.*[25] build on the work of Brechbühler *et. al.*[26] and use the parameterization of a closed surface onto a unit sphere with relative mesh triangle area and angle preservation to establish correspondence at a set of regular points in angular parameter space. We use a combination of the above works, further developed to analyse radiotherapy structure delineations.

3. GENUS ZERO SURFACE PARAMETERISATION

A two dimensional contour can be parameterised in terms of the distance of a point around the contour as a fraction of the total perimeter length. When this measure is taken as a fraction of 2π radians, the contour can be thought of as being mapped onto a unit circle, with the contour perimeter Cartesian coordinates becoming a function of the polar angle. The contour can then be analysed using Fourier descriptors, a well known and used technique in the field of shape analysis[27, 28]. Correspondence points are established at arbitrary points in parameter space (i.e. at arbitrary points around the unit circle) from a common origin, allowing the creation of a classic two dimensional point distribution model[20].

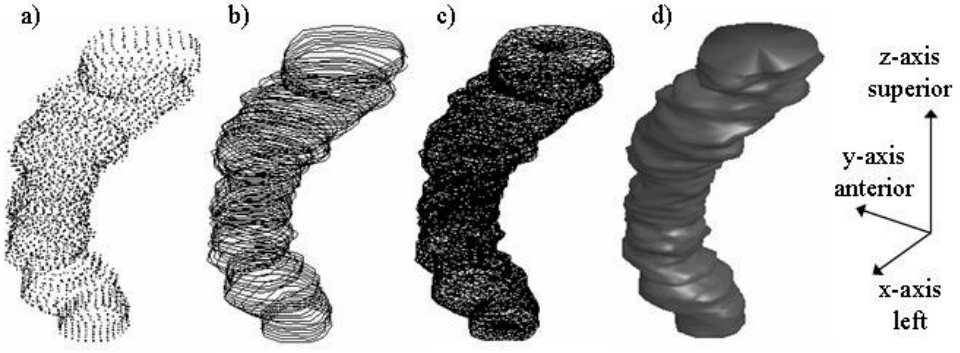

Figure 1 - A collection of discrete points (a) that make up a three dimensional medical image delineation, this is a rectum from a time-of-treatment CBT dataset. The points are connected in some way that enables the structure to be displayed to screen, this is often as a series of parallel plane contours (b) but may be as a three dimensional polygonal mesh (c) that can be rendered using raytracing techniques (d). The axes show the external machine coordinates and anatomical directions.

The three dimensional analogue of parameterising a closed contour onto a circle is the parameterisation of a genus zero closed surface onto a unit sphere, the three Cartesian coordinates becoming functions of the spherical angles. The preservation of geodesic distance about the contour as a fraction of the total length of the contour is replaced with the preservation of relative area as a fraction of the total surface area. As in two dimensions, correspondence points are established at regular points in parameter space, aligning the parameterisation coordinates taking the place of choosing a common origin.

A medical image delineation is a series of discrete points scattered throughout a three dimensional volume with some connectivity between them. Often these are a series of contours in the axial plane (x-y plane in the radiotherapy external machine quoted in out figures) with each point in the contours assumed to be connected to the next in a linear fashion, although some delineation algorithms work directly with a three dimensional polygonal mesh. Figure 1 shows various representations of the same rectal delineation on a CBT dataset. The parameterisation of meshes onto a sphere is a young and active research area, albeit well known. A genus zero closed surface can always be parameterised onto a sphere using either conformal (angle preserving) or equiareal (area preserving) techniques[29-31].

Brechbühler uses a diffusion model to map a mesh onto the unit sphere, here a vertex is chosen as the 'north' pole and another as the 'south', the south pole is given a value of π radians, the north 0 radians and a discrete Laplace equation solved to find the latitude of each vertex in the mesh. To find the longitude an arbitrary 'dateline' is created between the north and south vertices and a cyclic Laplace equation solved, with the longitude being incremented by 2π radians if a connection moves to the 'east' off the dateline and decremented by the same amount for moving 'westward' onto the dateline[26]. We follow this technique to obtain an initial approximation of the mapping and then use a global optimisation routine to minimize relative area and angular distortion of the now spherical triangles of the mesh. The objective function we have chosen uses a combination of equiareal and conformal factors, summing the square difference of the spherical and mesh relative triangle areas together with the square difference of spherical and mesh triangles' three relative side lengths (as a fraction of their perimeter length):

$$f = a\sum_{i=1}^{N}\left(\frac{A_i^{sphere}}{4\pi} - \frac{A_i^{mesh}}{\sum_{j=1}^{N} A_j^{mesh}}\right) + (1-a)\sum_{i=1}^{N}\sum_{j=1}^{3}\left(\frac{l_{ji}^{sphere}}{P_i^{sphere}} - \frac{l_{ji}^{mesh}}{P_i^{mesh}}\right) \quad (1)$$

Here A_i^{sphere} is the area of the ith spherical triangle and A_i^{mesh} is the area of the ith planar triangle in the surface mesh; l_{ji}^{sphere} is the length of the jth side of the ith spherical triangle, l_{ji}^{mesh} the length of the jth side in the ith planar mesh triangle, P_i^{sphere} and P_i^{mesh} are the perimeter length of the ith spherical and planar triangles respectively. The relative weight of the equiareal and conformal contributions to the function is controlled by the 'a' parameter. There are N triangles in the mesh.

We also impose constraints of 3 radians on the vertex angles to prevent triangle flipping, this is reasonable in the context of none of the original polygon mesh triangles having highly obtuse angles. A solution is sought using the Numerical Algorithms Group non-linear constrained optimisation routine e04ugg[32]. The global approach used by Brechbühler[26] and ourselves has inherent problems associated with it in that optimisation is computationally very expensive for large meshes consisting of several thousand vertices and the existence of local minima that can distort the final optimisation. Quicken *et. al.*[33] use a multi-resolution optimisation, where the mesh is decimated through some levels, optimised and then re-populated with the removed triangles, re-optimising at every level. This approach can speed up the process and help to remove the local minima.

It has been found by the authors of this paper that the choice of 'poles' can have an unexpectedly significant impact on how close the initial parameterisation is to one which is optimal. Figure 2 illustrates the point by showing the results of choosing either those vertices separated by the greatest Euclidean distance in object space or those that close a series of co-planar contours. We choose the closing vertices of the most superior and inferior contours, resulting in an ordered parameterisation that reaches the optimisation conditions much faster than other cases, and is less prone to errors. CBT delineations are generally composed of many more axial contours than ones based on a traditional planning CT scan due to the increased resolution along the inferiosuperior axis. To further improve parameterisation computational speeds where necessary, contour averaging can be employed to reduce the number of vertices in the mesh.

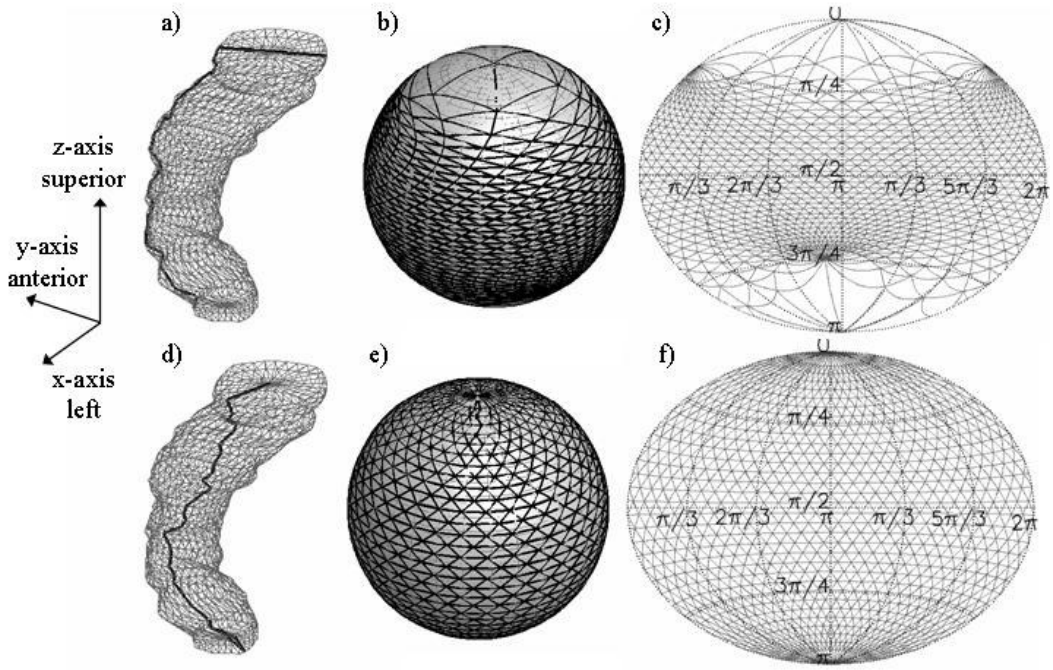

Figure 2 – The choice of 'poles' on a genus zero polygon mesh can significantly affect the initial parameterisation. Choosing the closing vertices of an axial delineation (d) results in a dateline roughly orthogonal to the contours (thick line on wireframe) with a resulting ordered parameterisation (e and f). If the poles are taken to be the vertices with the greatest Euclidean separation (a) the initial parameterisation will require greater optimisation. The data shown here is the same as that in Figure 1.

4. CREATION OF CORRESPONDENCE POINTS

To establish correspondence points, the parameter nets must first be commonly aligned, since after optimisation they are rotated at some arbitrary angle to each other. Both Quicken *et. al.*[33] and Kelemen *et. al.*[25] use the system proposed by Brechbühler[26] which makes use of the fact that the three sets of parameterised Cartesian coordinates form functions over the surface of the sphere. It is well known that any piecewise continuous function over some closed interval, [a,b], can be expanded in terms of a complete set of orthogonal functions, namely a generalised Fourier series. The spherical harmonics, the angular solution of the Laplace equation, form such a system and as such can be used to expand a function over the surface of a sphere, this particular harmonic expansion is sometimes thus known as the Laplace series[34-37]:

$$f(\theta,\phi)=\sum_{\ell=0}^{\infty}\sum_{m=-\ell}^{\ell}c_{\ell}^{m}Y_{\ell}^{m}(\theta,\phi) \qquad \begin{matrix}\theta\in[0,\pi]\\ \phi\in[0,2\pi)\end{matrix} \qquad (2)$$

Here $Y_{\ell}^{m}(\theta,\phi)$ are the spherical harmonics and c_{ℓ}^{m} are the harmonic coefficients expanding the function $f(\theta,\phi)$ with θ and ϕ the polar and azimuthal angles respectively. The series is hierarchical, low order expansions approximating the gross variability of the function with successively higher frequency information added as more terms are added. If the three coordinate functions over the sphere are expanded to only the first order ($\ell=1$), the resulting shape is an ellipsoid approximating the coarse elongation of the parameterised object in object space (see Figure 3). The method then depends upon an assumption that the first order expansions of similar shapes will result in ellipsoids with the same (or very similar) elongation. By rotating the parameter nets on the unit sphere until they have a common distribution on the first order ellipsoids, the parameter systems are aligned and any point in parameter space can be taken as a correspondence point.

This method, however, fails for structures such as the rectum where there is only one obvious axis. Figure 3 shows how when viewed along the major axis, there is often no distinct minor axis; this makes it possible to align the latitude of the parameterised vertices by placing a pole at one end of the major axis but impossible to align the longitudes correctly.

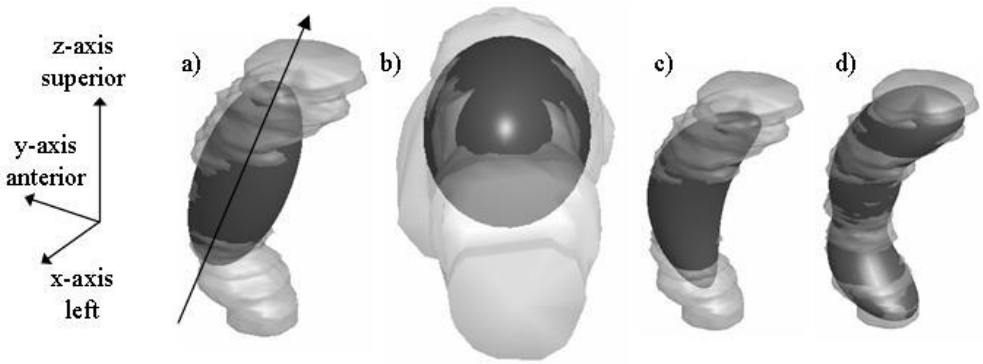

Figure 3 – The first order Laplace series expansion of an object parameterised onto a sphere results in an ellipsoid approximating the elongation of the parameterised object (a), the major axis of the ellipsoid is indicated by the arrow. Viewing the ellipsoid along the major axis (b), however, shows that for some objects, such as the rectum shown here, there is not sufficient difference in the orthogonal object elongations to make the minor axis distinct, the object tends towards being a spheroid. (c) and (d) show the second and fifth order Laplace series expansions of the rectum delineation respectively with the expansion becoming closer to the original shape.

We use two landmarks to align the parameterised rectal delineations. One is placed at the anus, which is relatively immobile, and serves to align the latitudes, the other is placed at the fatty tissue pad where the prostate and rectum are closest and is used to align the longitudes correctly (Figure 4). The closest points on the delineation to the landmarks are calculated via optimisation of the Euclidean distance from them to the points within each mesh triangle described by their parametric equations. The same calculation hence yields the barycentric coordinates of the closest points allowing their parameterisation via a simple weighted trilinear interpolation.

5. ANALYSIS OF CORRESPONDING POINTS

The simplest method to describe the variability of shapes once correspondence points have been established is to treat each point in parameter space individually. In the case of polar shapes, where correspondence is immediately established from a common origin as a function of the spherical angles, each correspondence point reduces to a simple one dimensional analysis of the radial distance from the origin as described thoroughly by Remeijer *et. al.*[22]. However, where a shape has been parameterised as described in Section 4, the correspondence points will result in a 'vertex cloud' in three dimensions. This can be analysed in exactly the same manner, breaking the cloud into three orthogonal components. These could be taken using the external radiotherapy machine coordinate system or in relation to the surface normal of the mean shape. A total of four maps would then have to be displayed, one showing the variability in each of the three orthogonal axes and the other the overall magnitude of the variability.

In their 1995 paper Cootes *et. al.* assume that each set of corresponding vertices do not move independently of each other, being partially correlated in some way[20]. There are three degrees of translational freedom at each correspondence point and thus a set of N shapes can be represented as a point cloud in 3n dimensional space if there are n points. Applying principal component analysis (PCA) to this 3n dimensional space, the major modes of variability can be found. Instead of using the direct point data, Kelemen *et. al.* analyse the variability of the Laplace series coefficients, again using a PCA approach to find the major modes of variability[25]. In both cases the modes of variability are created from a mean shape. This can be used, as both Cootes *et. al.* and Kelemen *et. al.* do, to create a statistical shape model where the major modes of variation are

balanced against some image information to automatically segment a grey-level image. Alternatively, we propose, a variability map can be created by tracing the displacement of the correspondence points.

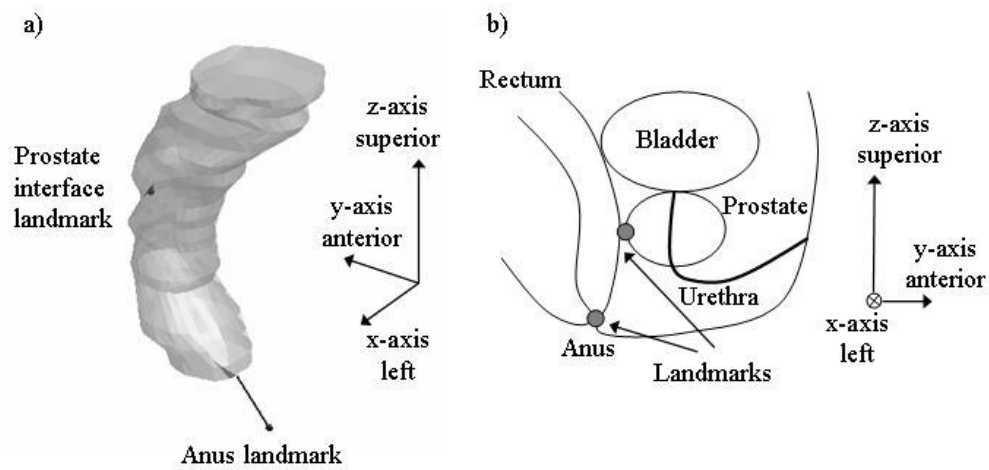

Figure 4 – Transparent raytracing of rectal delineation together with the relative positioning of two landmarks (a), the anus and prostate/rectum interface. The lines point to the closest point on the surface of the mesh to the landmarks, the mesh triangles that contain these points are shown in a darker shade. These points are parameterised via a spherical interpolation of the latitude and longitude of the surrounding vertices. An anatomical diagram of the region is also shown (b). The average inferiosuperior distance between the landmarks is ~65mm to provide a scale for the image.

6. CASE STUDY

At the Christie hospital, patients are being selected to receive time-of-treatment 3D CBT scans during some or all of their treatment fractions as part of the emerging image guided radiotherapy (IGRT) programme. This study uses a set of 16 CBT scans from a male prostate cancer patient taken serially over his entire fractionation schedule of 3 weeks. The rectum was delineated in each image set by between 2 to 4 observers, a mixture of research clinicians and radiographers, with the total number of delineations standing at 45.

Figure 5 shows the overall observer variability for the entire dataset. The population variability was estimated for each image set, treating each component (in external machine coordinates) of each correspondence point as a one dimensional statistical problem, in the usual way and averaged over all the imagesets:

$$s = \sqrt{\frac{1}{\sum_{j=1}^{N}(n_i - 1)} \sum_{i=1}^{N} \sum_{j=1}^{n_i} \left(r_{i,j} - \bar{r}_i\right)^2} \qquad \begin{array}{c}\text{Imagesets, } i = 1 \rightarrow N \\ \text{Observers, } j = 1 \rightarrow n_i\end{array} \qquad (3)$$

Where r is the correspondence point coordinate in object space, N is the total number of imagesets and n_i is the number of observers from the ith imageset. The magnitude at each point is calculated as the norm of the separate coordinate components. This statistic actually contains both the inter- and intra-observer variability, the sparseness of this particular dataset preventing their separation.

Once the nature of the observer variability is known, it is possible to create maps showing the deviation from the mean required at each correspondence point in order for the change to be considered significant. Assuming that the distribution of the observer variability is normal[24], the standardized deviate can be calculated for any arbitrary significance level. The two

tailed deviates for significance levels of P=0.05 and P=0.01 are 1.96 and 2.58 respectively. As there are many correspondence points over the surface, there is an expectation that some number of points (5% and 1% respectively) will show significant deviations by chance. Applying the Bonferroni correction[38, 39] adjusts the probability level to take account of this; the two tailed deviates for significance levels of P=0.05 and P=0.01 with 1800 correspondence points are 4.19 and 4.54.

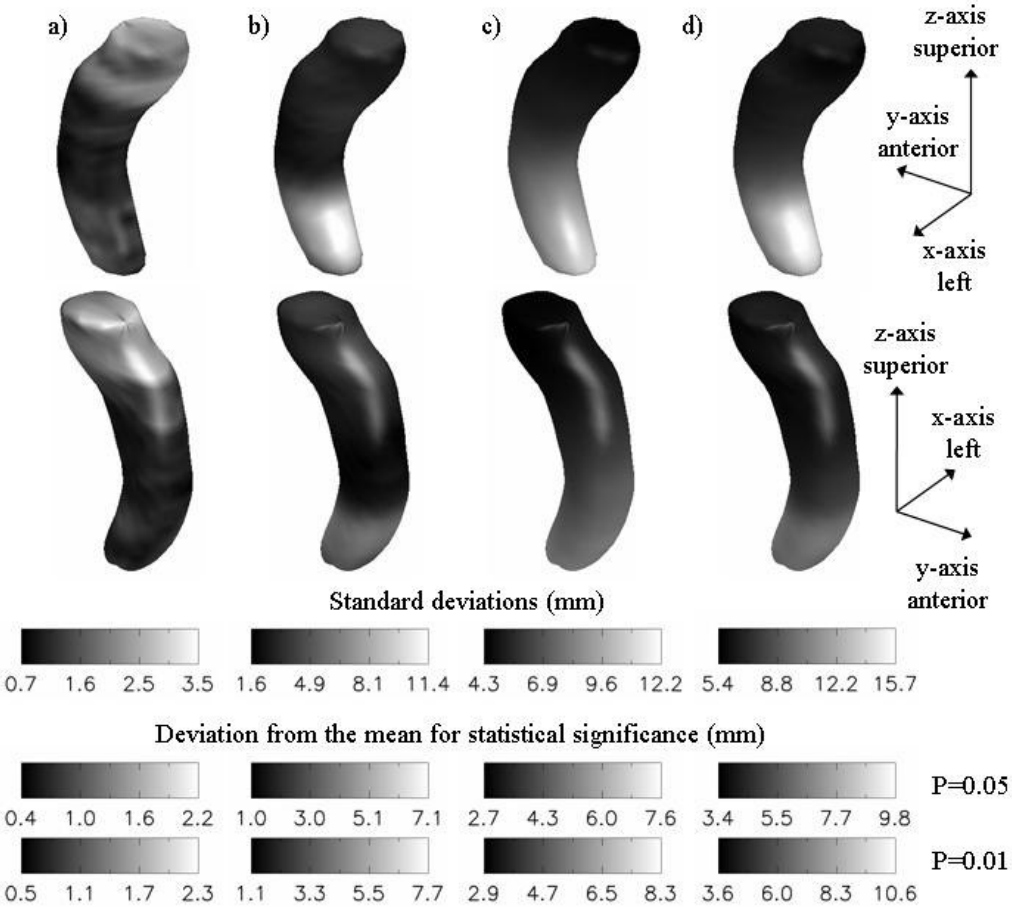

Figure 5 – The overall observer standard deviations. (a) shows the x component, (b) the y component, (c) the z component and (d) the magnitude of the variability at each correspondence point established in parameter space. The delineation shows the overall mean surface over the 16 image sets. The deviation from the mean required for a particular significance level is proportional to both the standardized deviate and the standard error and hence will have the same distribution as the variability. The additional colour bars below the standard deviation show the deviation required to be considered significant and the P=0.05 and P=0.01 levels for the different components, including the Bonferroni correction. The position of the rectum delineation relative to the prostate and anus is shown in Figure 4.

The deviate varies linearly with deviation from the mean and in inverse proportion to the standard error of the mean (Table 1), hence the variability, standard error and deviation will all have the same distribution. Figure 5 shows the deviations required from the mean to be considered statistically significant, within this dataset, to a level of P=0.05 or P=0.01. The authors acknowledge that this analysis assumes that the population mean and variance are known, whereas of course they have only been estimated from a sample of this, however, we believe it to be sound when comparing means which themselves for a subset of this data.

Variability component	x	Y	z	Magnitude
Standard error (mm)	0.11 → 0.52	0.24 → 1.69	0.64 → 1.81	0.80 → 2.34

Table 1 – The range of the standard error of the mean surface. The distribution will be as for the variability shown in Figure 5.

Figure 6 shows the variability of the mean surfaces generated from the CBT scan taken at each treatment fraction. Figure 7 shows the percentage of the mean surfaces that deviate from the overall mean surface by more than the P=0.01 statistically significant amount shown in Figure 5.

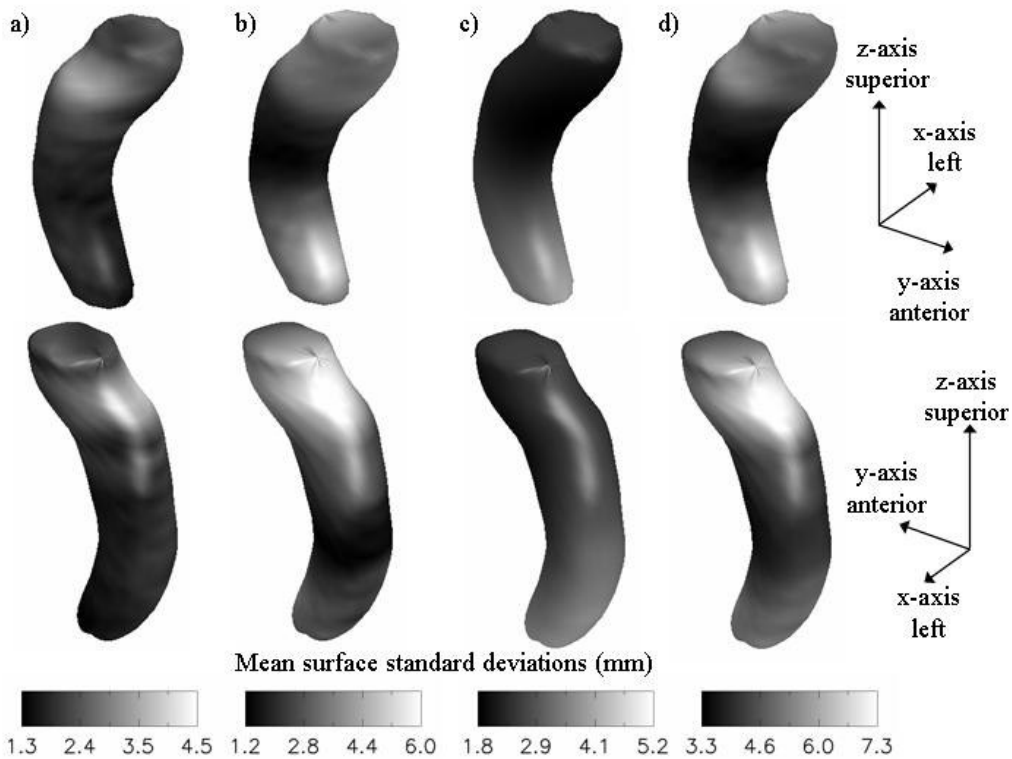

Figure 6 – The standard deviations of the mean for each imageset (fraction date) about the overall mean surface. (a) shows the x component, (b) the y component, (c) the z component and (d) the magnitude of the variability at each correspondence point.

Typical values for the one dimensional overall observer variability previously quoted in the literature are: 0.0mm→3.6mm (prostate)[22], 0.0mm→2.5mm (bladder)[40] and 0.0mm→2.1mm (bladder)[24]. The variability magnitudes in Figure 5 are higher than this, although the very large values are dominated by the y and z components towards the inferior end of the delineation. This is broadly due to different outlining methods employed by the different observers with some continuing much further towards the anus (i.e. in the negative z direction) that others. As the rectum tends to curve in an posterior direction as it approaches the anal canal, a higher y component variability would also be expected. With a sufficient contouring protocol in place, this would be eliminated.

The distribution for the standard deviation of the mean surface over the fractionation schedule (Figure 6) is markedly different to that of the observer variability, with the maximum variation seen at the superior end of the structure, especially in the y component. Figure 7 shows that lateral (i.e. x component) variability is significant, with respect to the overall observer variability, over the entire structure although quite small in scale. There is little significant z component movement, but large (up to 6mm), and statistically significant, movement is seen in the anteroposterior (i.e. y component) direction at the superior

end of the anterior wall. It is this motion that is of great concern during the treatment of disease in the pelvic region as the target region can be shifted out of the beam path and OARs into it.

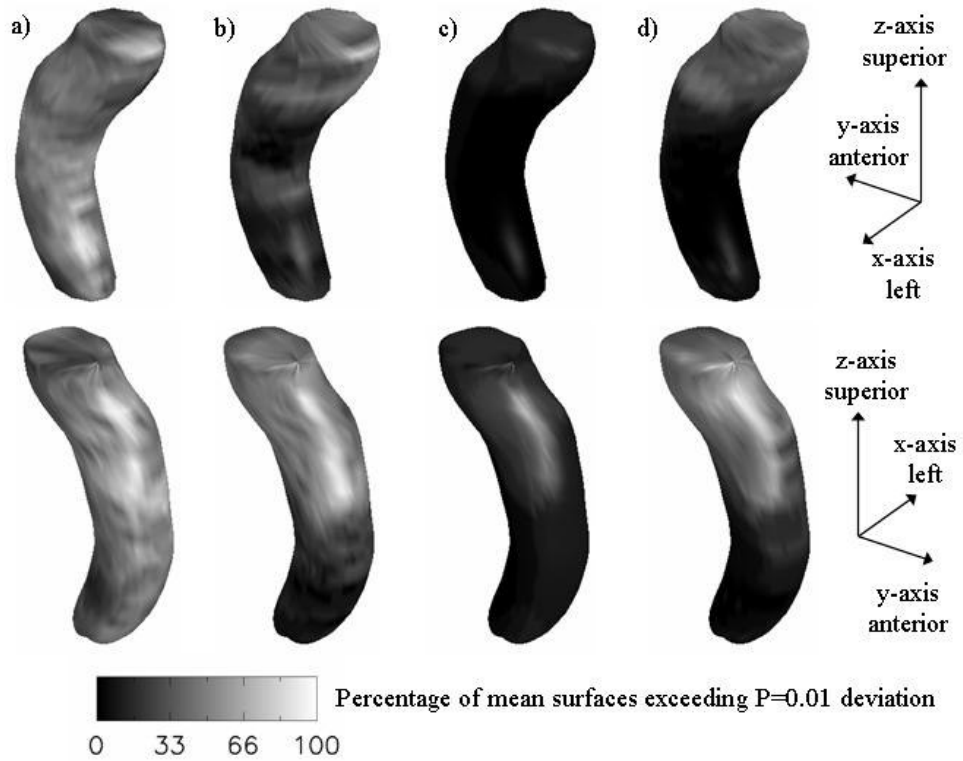

Figure 7 – The percentage of the mean surfaces generated for each imageset that exceed the P=0.01 significance deviations from the overall mean given in Figure 5 (including Bonferroni correction). (a) shows the x component movement, (b) the y component, (c) the z component and (d) the magnitude.

7. DISCUSSION

The case study presented in Section 6 uses a simple technique to show where significant motion of the rectum is seen over the 16 treatment fractions for one patient. The analysis is based upon several reasonable and highly practical assumptions: that the inter- and intra-observer variability is normally distributed, that the observers are representative of the population of observers and that the mean surfaces created for each scan imageset are normally distributed about an unchanging overall mean.

The case study highlights the methodology, further studies are planned to produce more extensive datasets at a wider range of anatomical sites. With a bigger and more complete dataset, including multiple delineations by the same observer on each imageset (to allow the separation of the inter- and intra-observer effects from the overall observer variability) a more complex mixed effects statistical model could be used. This could be used to test if there were any effect upon the mean surface as a function of time rather than assuming it is constant – it seems possible that during treatment there will be some effect upon not only the target but also on the OAR.

8. CONCLUSIONS

A method of using quantitative statistics to measure the variability of non polar radiotherapy delineations has been presented. This technique has been used to show, in a small case study, that statistically significant movement of the rectal walls over the period of one patient's fractionation schedule are observed. The use of evidence based points, polar selection, minimal landmarking that is relevant to the anatomy being investigated and intuitive displays of results in 3D makes the use of advanced analyses of shape more accessible to the clinical community.

As image guided radiotherapy becomes more common place, large numbers of complete image datasets tracing a patient's progress through treatment ,with the associated delineation libraries, will become available. It is the authors' hope that this data can be processed, using this and similar techniques, to eventually yield statistically robust models of population organ motion and how this motion responds to radiation therapy. This will allow the definition of evidence based non-uniform error margins that will help to spare healthy tissue from unnecessary radiation exposure whilst ensuring the entire target area receives the correct tumourcidal dose.

9. ACKNOWLEDGEMENTS

This work was supported by the United Kingdom Engineering and Physical Sciences Research Council (EPSRC) grant number GR/S41340/01. We thank R. Sripdam, P. Jain, A. Henry and J. Stratford for providing the delineations used in this study.

10. BIBLIOGRAPHY

1. C. Rasch *et. al.*, "Target definition in prostate, head, and neck", Seminars in Radiation Oncology, **15** (3) p136-45 (2005)
2. L.F. Cazzaniga *et. al.*, "Interphysician variability in defining the planning target volume in the irradiation of prostate and seminal vesicles", Rad.Oncol., **47** (3) p293-296 (1998)
3. C. Fiorino *et. al.*, "Intra- and inter-observer variability in contouring prostate and seminal vesicles: implications for conformal treatment planning", Rad.Oncol., **47** (3) p285-292 (1998)
4. C.S. Hamilton and M.A. Ebert, "Volumetric Uncertainty in Radiotherapy", Clinical Oncology, **17** (6) p456-464 (2005)
5. M. Roach, 3rd *et. al.*, "Prostate volumes and organ movement defined by serial computerized tomographic scans during three-dimensional conformal radiotherapy", Radiation Oncology Investigations, **5** (4) p187-194 (1997)
6. S. Shimizu *et. al.*, "Impact of respiratory movement on the computed tomographic images of small lung tumors in three-dimensional (3D) radiotherapy", International Journal of Radiation Oncology Biology and Physics, **46** (5) p1127-1133 (2000)
7. J.M. Balter *et. al.*, "Measurement of prostate movement over the course of routine radiotherapy using implanted markers", International Journal of Radiation Oncology Biology and Physics, **31** (1) p113-118 (1995)
8. T.E. Byrne, "A review of prostate motion with considerations for the treatment of prostate cancer", Medical Dosimetry, **30** (3) p155-161 (2005)
9. "ICRU Report 62: Prescribing, recording and reporting photon beam therapy (supplement to ICRU Report 50)", International Commission on Radiation Units and Measurements, Report - 62, (1999)
10. "ICRU Report 50: Prescribing, recording and reporting photon beam therapy", International Commission on Radiation Units and Measurements, Report - 50, (1993)
11. E. Astreinidou *et. al.*, "Adequate margins for random setup uncertainties in head-and-neck IMRT", Int.J.Rad.Oncol.Biol.Phys, **61** (3) p938-944 (2005)
12. J.C. Stroom and B.J.M. Heijmen, "Geometrical uncertainties, radiotherapy planning margins, and the ICRU-62 report", Rad.Oncol., **64** (1) p75-83 (2002)
13. M. van Herk, "Errors and margins in radiotherapy", Seminars in Radiation Oncology, **14** (1) p52 (2004)

14. M. Roach, 3rd, "Commentary on increased risk of biochemical and local failure in patients with a distended rectum on the planning CT for prostate cancer radiotherapy", Int.J.Rad.Oncol.Biol.Phys, **62** (4) p949-50 (2005)
15. R. de Crevoisier *et. al.*, "Increased risk of biochemical and local failure in patients with distended rectum on the planning CT for prostate cancer radiotherapy", Int.J.Rad.Oncol.Biol.Phys, **62** (4) p965-73 (2005)
16. C.A. McBain *et. al.*, "X-ray volumetric imaging in image-guided radiotherapy: The new standard in on-treatment imaging", Int.J.Rad.Oncol.Biol.Phys, **In Press, Corrected Proof**
17. S. Marshall, "Review of shape coding techniques", Im.Vis.Comp., **7** (4) p281-294 (1989)
18. B.M. Mehtre *et. al.*, "Shape measures for content based image retrieval: A comparison", Inf.Process.Manag., **33** (3) p319-337 (1997)
19. J.W.H. Tangelder and R.C. Veltkamp, "A survey of content based 3D shape retrieval methods", *in Proceedings of the Shape Modeling Applications 2004,*p145-156 Pub: IEEE Computer Society, Genova, Italy (2004)
20. T.F. Cootes *et. al.*, "Active Shape Models - Their Training and Application", Comp.Vis.Im.Und., **61** (1) p38-59 (1995)
21. A. Caunce and C.J. Taylor, "3D point distribution models of the cortical sulci", *in Proceedings of the Sixth International Conference on Computer Vision,*p402-407 Pub: IEEE, (1998)
22. P. Remeijer *et. al.*, "A general methodology for three-dimensional analysis of variation in target volume delineation", Medical Physics, **26** (6) p931-940 (1999)
23. G.J. Price and C.J. Moore, "A simple polar parameterisation method to show quantitative spatial variation between delineations on medical image datasets", *in Proceedings of the Medical Information Visualisation,*p47-55 Pub: IEEE Computer Society, Greenwich, London (2005)
24. K.E. Deurloo *et. al.*, "Quantification of shape variation of prostate and seminal vesicles during external beam radiotherapy", Int.J.Rad.Oncol.Biol.Phys, **61** (1) p228-38 (2005)
25. A. Kelemen *et. al.*, "Elastic model-based segmentation of 3-D neuroradiological data sets", IEEE.Trans.Med.Im., **18** (10) p828-839 (1999)
26. C. Brechbühler *et. al.*, "Parameterisation of closed surfaces for 3-D shape description", Comp.Vis.Im.Und., **61** (2) p154-170 (1995)
27. E. Persoon and K.S. Fu, "Shape Discrimination Using Fourier Descriptors", IEEE Transactions on Systems Man and Cybernetics, **7** (3) p170-179 (1977)
28. C.T. Zahn and R.Z. Roskies, "Fourier Descriptors for Plane Closed Curves", IEEE Transactions on Computers, **C 21** (3) p269-281 (1972)
29. M.S. Floater and K. Hormann, "Surface Parameterization: a Tutorial and Survey", *in Proceedings of the Advances in Multiresolution for Geometric Modelling,*p157-186 Pub: Springer, Berlin, Heidelberg (2005)
30. E. Praun and H. Hoppe, "Spherical Parameterization and Remeshing", ACM.Trans.Graph., **22** (3) p340-349 (2003)
31. C. Gotsman *et. al.*, "Fundamentals of spherical parameterization for 3D meshes", ACM.Trans.Graph., **22** (3) p358-363 (2003)
32. The Numerical Algorithms Group, *NAG C library introductary guide, mark 7*, NAG (2002)
33. M. Quicken *et. al.*, "Parameterization of Closed Surfaces for Parametric Surface Description", *in Proceedings of the Computer Vision And Pattern Recognition,*pI-354-I-360 Pub: IEEE Computer Society, (2000)
34. G.B. Arfken and H.-J. Weber, *Mathematical methods for physicists*, 4th ed., Academic Press (1995)
35. H. Groemer, *Geometric applications of Fourier series and spherical harmonics*, Cambridge University Press (1996)
36. E.W. Hobson, *The theory of spherical and ellipsoidal harmonics*, Cambridge University Press (1931)
37. R. Courant and D. Hilbert, *Methods of mathematical physics*, Interscience (1953)
38. R.S.J. Frackowiak *et. al.*, *Human brain function*, 2nd ed., Academic Press (2003)
39. P. Armitage *et. al.*, *Statistical methods in medical research*, Blackwell Science (2002)
40. G.J. Meijer *et. al.*, "Three-dimensional analysis of delineation errors, setup errors, and organ motion during radiotherapy of bladder cancer", Int.J.Rad.Oncol.Biol.Phys, **55** (5) p1277-1287 (2003)